

Nanoscale

Accepted Manuscript



This is an *Accepted Manuscript*, which has been through the Royal Society of Chemistry peer review process and has been accepted for publication.

Accepted Manuscripts are published online shortly after acceptance, before technical editing, formatting and proof reading. Using this free service, authors can make their results available to the community, in citable form, before we publish the edited article. We will replace this *Accepted Manuscript* with the edited and formatted *Advance Article* as soon as it is available.

You can find more information about *Accepted Manuscripts* in the [Information for Authors](#).

Please note that technical editing may introduce minor changes to the text and/or graphics, which may alter content. The journal's standard [Terms & Conditions](#) and the [Ethical guidelines](#) still apply. In no event shall the Royal Society of Chemistry be held responsible for any errors or omissions in this *Accepted Manuscript* or any consequences arising from the use of any information it contains.

High-sensitive Eu^{3+} ratiometric thermometers based on excited state absorption with predictable calibration

5 *Adelmo S. Souza,^{a*} Luiz A. O. Nunes,^b Ivan G. N. Silva,^c Fernando A.M. Oliveira,^b Leonis
L. da Luz,^a Hermi F. Brito,^c Maria C. F. C. Felinto,^d Rute A. S. Ferreira,^e Severino A. Júnior,^a
Luís D. Carlos,^{e*} Oscar. L. Malta^a*

^a Departamento de Química Fundamental-CCEN-UFPE, Cidade Universitária, Recife-PE,
10 50670-901, Brazil

^b Instituto de Física de São Carlos, Universidade de São Paulo - USP, CEP 13560-970, São
Carlos - SP, Brazil

^c Instituto de Química, Universidade de São Paulo, 05508-900 São Paulo - SP, Brazil

^d Centro de Química do Meio Ambiente, Instituto de Pesquisas Energéticas e Nucleares, Av.
15 Prof. Lineu Prestes, 2242, SP, 05508-000 São Paulo - SP, Brazil

^e Department of Physics and CICECO Aveiro Institute of Materials, University of Aveiro,
3810–193 Aveiro, Portugal

* Correspondence to: Dr A. S. Souza, E-mail: adelmosaturnino@hotmail.com; Prof. L. D.
20 Carlos, E-mail: lcarlos@ua.pt

Abstract

Temperature measurements ranging from few degrees to few hundreds degrees Kelvin are of large interest in the fields of nanomedicine and nanotechnology. Here, we report a new
5 radiometric luminescent thermometer using thermally excited state absorption of the Eu^{3+} ion. The thermometer is based on the simple Eu^{3+} energy level structure and can operate between 180 and 323 K with a relative sensitivity ranging from 0.7 to 1.7 % K^{-1} . The thermometric parameter is defined as the ratio between the emission intensities of the ${}^5\text{D}_0 \rightarrow {}^7\text{F}_4$ transition when the ${}^5\text{D}_0$ emitting level is excited through the ${}^7\text{F}_2$ (physiological range) or the ${}^7\text{F}_1$ (down
10 to 180 K) level. Nano and microcrystals of $\text{Y}_2\text{O}_3:\text{Eu}^{3+}$ were chosen as a proof of concept of the operational principles in which both excitation and detection are within the first biological transparent window. A novel and of paramount importance aspect is that the calibration factor can be calculated from the Eu^{3+} emission spectrum avoiding new calibration procedures whenever the thermometer operates in different media.

15

Keywords: Eu^{3+} luminescence thermometers, excited state absorption, Y_2O_3 , predictable calibration

Introduction

Temperature is a fundamental thermodynamic parameter, the measurement of which is crucial in numerous scientific investigations and technological developments, accounting at present for 80% of the sensor market throughout the world.¹⁻³ The majority of these sensors require direct contact with the body we are trying to measure and, therefore, ineffective for precise temperature measurements at the submicron scale, *e.g.*, in semiconductor junctions in microelectronics^{4, 5} and intracellular mappings in nanomedicine.^{6, 7} This intrinsic limitation has encouraged the development of non-invasive accurate thermometers with micrometric and nanometric resolution, such as infrared (IR) and luminescence thermometers, a challenging research topic increasingly hankered for.⁸⁻¹⁵ However, although IR cameras are commonly used in thermometry they present the following disadvantages: i) limited spatial resolution (typically, >100 μm); ii) previous knowledge of the material surface emissivity (that is function of wavelength and temperature); iii) considerable temperature uncertainty (~ 2 degree at room temperature, acceptable values only above 318 K) and iv) strong dependence on the relative orientation between the camera and the measured surface.^{16, 17} Moreover, in biological samples due to the presence of water the estimation of the emissivity and thus of the temperature is very difficult. Then, conventional IR thermometry is not able to give reliable and meaningful temperature readouts being ratiometric luminescent thermometers a much more reliable approach for precise temperature measurements with high detection sensitivity, spatial and temperature resolution and short acquisition times.¹⁸

Although relatively recent (luminescent thermometry exploded over the past five years), the technique appears to be beneficial to many technological applications in a great variety of areas, such as microelectronics, microfluidics, bio- and nanomedicine. In the particular case of bio- and nanomedicine, accurate temperature sensing is crucial because temperature is one of the most critical factors affecting the dynamics of living specimens.^{7, 19-21}

The luminescent thermometers developed up to now encompass organic dyes,^{22, 23} polymers,²⁴ quantum dots²⁵ (QDs) and Ln³⁺ ions^{1, 3, 8, 12, 13, 26-29} as the optically active centers. The bleaching of the organic dyes and the QDs under continuous illumination is a drawback limiting its use. Moreover, the size distribution of the QDs (that leads to a non-homogeneous luminescence individual response) and its poor solubility, agglutination, instability in different environments, and toxicity to biological systems are also limitations.^{30, 31} Concerning the thermometers based on fluorescence polymers, a typical limitation is the hysteresis, *i.e.*, differences in the output, for the same temperature value, depending on if the temperature is increasing or decreasing.²³ This translates to an error in the temperature determination that may extend into a relevant fraction of the operation range. The limited operating range due to thermally-activated structural conformational changes is also a significant constrain.¹

Among the Ln³⁺-based luminescent thermometers four general families (one non-ratiometric) have been considered in the literature: i) Eu³⁺-based materials (non-ratiometric),^{9, 32} upconversion co-doped micro and nanocrystals (involving essentially Yb³⁺ and Er³⁺),³³⁻³⁵ iii) near infrared (NIR) excited downshifting Nd³⁺-based materials;^{11, 17, 36-39} and iii) UV excited downshifting Tb³⁺/Eu³⁺ co-doped systems.^{8, 13, 18, 40}

All of these examples have disadvantages. For instance, upconversion is a rather low inefficient process requiring the use of high power excitation sources that induce a local heating making difficult to evaluate the real temperature of the system. Moreover, the relative sensitivity S_r of the thermometers reported so far – a parameter used as a figure of merit to compare the performance of different systems –¹ is always low (typically $\sim 1-2 \text{ \%}\cdot\text{K}^{-1}$). Concerning the Nd³⁺-based thermometers, although both excitation and detection are within the first biological transparency window, an advantage for biological applications, the relative sensitivity is quite low (typically $\sim 10^{-1} \text{ \%}\cdot\text{K}^{-1}$),¹⁷ as, generally, the temperature is measured through the relative intensity between two Stark components.³⁹ Typically, the relative

temperature variation of the thermometric parameter in the physiological range (298–323 K) is lower than 10%.¹ UV-excited Tb³⁺/Eu³⁺ luminescent thermometers suffers from several drawbacks relatively to those operating through NIR excitation, as the much smaller penetration depth, $\sim 10^{-2}$ m, high damaging to cells (especially when high-power densities are used), and signal measurements disturbed by tissue autofluorescence. In contrast, its relative sensitivity is larger ($>1 \text{ \%}\cdot\text{K}^{-1}$).⁸ An important point is that all of these systems require a previous calibration of the temperature dependence of the thermometric parameter. This might be a limitation when the thermometers are used in a different medium than that in which they are calibrated.

Therefore, a crucial technological challenge is the development of a ratiometric luminescent thermometer that should have simultaneously the following requirements: i) high temperature and spatial resolution, $<0.1 \text{ K}$ and $<1 \text{ }\mu\text{m}$, respectively); ii) low excitation power ($<100 \text{ mW cm}^{-2}$) to avoid the local increase of the temperature due to radiation absorption; iii) high relative sensitivity, $>1 \text{ \%}\cdot\text{K}^{-1}$, iv) excitation and detection in wavelengths not strongly absorbed by biological tissues ($>580 \text{ nm}$), and v) an intrinsic calibration parameter that is dependent of well-known quantities and computable.

The usual calibration procedure requires an independent measurement of the temperature (using, for instance, a thermocouple or an IR camera) to allow its conversion to luminescence intensity ratio, implying that a new calibration procedure is required whenever the thermometer operates in a different medium. However, once this is not always possible (e.g., at the submicrometric scale) a single calibration is assumed to be valid independently of the medium. In this work, we overcome this bottleneck of luminescent thermometers using thermally populated low energy level excited state absorption in the trivalent europium ion (Eu³⁺) that permits the unprecedented prediction of the calibration factor. The new ratiometric luminescent thermometers proposed here fulfill the above listed requirements with exceptional advantages with respect to those reported so far. These are: 1) Once the

Souza et al.

calibration factor depends on easily obtainable spectroscopic quantities, it can be predicted; 2) Operating between 180 and 323 K, with a relative sensitivity ranging from 0.7 to 1.7 % K⁻¹ (>1.2 %·K⁻¹ in the physiological range), at least for concentrations up to 10 mol%; 3) No quenching effects due to cross relaxation and energy migration is operative in this concentration regime; 4) Sub-degree temperature resolution; 5) Excitation and detection in the 580–710 nm range (compatible with the optics and detection setup of the conventional fluorescent microscopes and cytometers), in which biological media do not strongly absorb; 6) Versatility, since it can be operative as micro and nanoparticles, films and powders; 7) Reproducibility higher than 97%.

10 These advantages are mainly due to the fact that the barycentre energy of the first and second excited states (⁷F₁ and ⁷F₂) lie at ~300 cm⁻¹ and ~1000 cm⁻¹, respectively, above the ⁷F₀ ground state. These three states turns out to be strongly coupled from the thermal point of view. The ⁷F₁ borrows considerable population from the ⁷F₀. Thus, at room temperature the thermal populations (in %) of the ⁷F₀, ⁷F₁ and ⁷F₂ states are 65%, 33% and 2%, respectively
15 (see equations 4 and 5 below), this is a unique feature of Eu³⁺ among the trivalent lanthanide ions. Although absorption from these latter two excited levels has been observed,⁴¹ no reference to the use of thermally Eu³⁺ excited state absorption in luminescence thermometry has been reported.

20 **Experimental**

Materials and Synthesis. Nanocrystals of Y₂O₃:Eu³⁺ (1 mol%) were synthesized previously by the benzenetricarboxylate method,⁴² whereas Y₂O₃:Eu³⁺ microcrystals (5 mol%) were provided by Osram Sylvania-Brazil. Transmission electron microscopy images (Fig. S1, Supporting Information) show that the prepared Y₂O₃:Eu³⁺ nanocrystals are formed
25 of agglomerates of individual crystallites at nanoscale with average size ranging from 5±1 nm

to 45 ± 9 nm, as the annealing temperature increases from 500 °C to 1000 °C, respectively. These values are very similar to those estimated from X-ray powder diffraction, using the Scherrer equation⁴² (see Supporting Information for details). The $\text{Y}_2\text{O}_3:\text{Eu}^{3+}$ nanocrystals annealed at 700 °C were selected for the photoluminescence studies.

5

Instrumental. The emission and excitation spectra of the two samples were obtained using an SPEX Fluorolog spectrofluorometer (0.22 m, Spex/1680) equipped with an Xe-lamp as the excitation source and a photomultiplier (Hamamatsu/R928) for detection. The emission spectra were corrected for the detection and optical spectral response of the spectrofluorometer and the excitation spectra were weighed for the spectral distribution of the lamp intensity using a photodiode reference detector. The spectra were taken at different temperatures by using a N_2 cryostat equipped with a temperature controller model 320 Autotuning (LakeShore).

15 **Results and Discussion**

The thermometer modeling is based on the schematic level diagram shown in Fig. 1, where W_{31} is the absorption rate from state 1 to state 3 and the intensity of the transition from level 3 to level 2 ($^5\text{D}_0 \rightarrow ^7\text{F}_4$ transition), I_{23} , is given by:

$$20 \quad I_{23} = \hbar\omega_{23}A_{23}N_3 \quad (1)$$

where N_3 is the population of level 3, A_{23} is the spontaneous emission rate from level 3 to level 2 and $\hbar\omega_{23}$ is the transition energy from level 3 to level 2.

25 **Insert Fig.1**

The rate equation for the population of level 3, N_3 , with lifetime τ_3 reads:

$$\frac{dN_3}{dt} = -\frac{1}{\tau_3}N_3 + W_{31}N_1 \quad (2)$$

5

The energy level 1 is very little depleted upon absorption (low power excitation). Thus, the population N_1 is by far dominated by the Boltzmann (thermal) population:

$$N_1 = p_1N \quad (3)$$

10

where N is the total number (per unit volume) of emitting ions and the Boltzmann population factor p_1 is:

$$p_1 = \frac{g_1 e^{-E_1/k_B T}}{Z} \quad (4)$$

15

Z is the partition function, given by:

$$Z = \sum_i g_i e^{-E_i/k_B T} \quad (5)$$

20 where g_i is the degeneracy of level i with energy E_i and k_B is the Boltzmann constant. In the steady state regime Eq. (2) equals zero and Eq. (1) reads:

$$I_{23} = \hbar\omega_{23}A_{23}\tau_3 p_1 W_{31}N \quad (6)$$

The idea is to define a ratiometric thermal parameter, Δ , by taking the ratio between the emission intensity I_{23} (${}^5D_0 \rightarrow {}^7F_4$), when the 5D_0 is excited through the 7F_2 , $I_{23}({}^7F_2)$, and through the 7F_0 , $I_{23}({}^7F_0)$, for the physiological range, or through the 7F_1 , $I_{23}({}^7F_1)$, and the 7F_0 , $I_{23}({}^7F_0)$ for low temperatures (down to 180 K). In the case of the physiological range the thermal parameter is given by:

$$\Delta = \frac{I_{23}({}^7F_2)}{I_{23}({}^7F_0)} = \frac{p({}^7F_2) W_{31}({}^7F_2)}{p({}^7F_0) W_{31}({}^7F_0)}. \quad (7)$$

The thermal parameter is experimentally determined measuring the areas under the emission curve, S , of the ${}^5D_0 \rightarrow {}^7F_4$ transition excited resonantly through the 7F_2 and the 7F_0 levels in the physiological temperature range. What is unique in this thermometer is that the thermal parameter can be predicted by the right hand side of Eq. (7). Both the ${}^7F_0 \rightarrow {}^5D_0$ and ${}^7F_2 \rightarrow {}^5D_0$ transitions are electric dipole in nature. Once the excitation power can be the same for both transitions and the emitting level 5D_0 and the ground state 7F_0 are nondegenerate, it is not difficult to conclude that the ratio between the absorption rates W_{31} in Eq. (7) may be given by the ratio between the areas under the emission curves of the ${}^5D_0 \rightarrow {}^7F_2$ and ${}^5D_0 \rightarrow {}^7F_0$ transitions under usual excitation from the ground state. It is important to note that this ratio does not depend on temperature, once, in this case, the thermal population of the 7F_0 ground state affects both transitions in the same manner. It is also important to note that the ratio between the absorption rates W_{31} cannot be extracted directly from the excitation spectrum, once the areas under the excitation curves obviously implicitly contain the temperature dependence whose analytical form we are interested in (we emphasize that the ratio between the W_{31} in Eq.(7) does not depend on temperature). It could be argued that the ratio between the absorption rates could be replaced by the ratio between the respective

oscillator strengths. However, this would require the use of 4f-4f intensity parameters and the J-mixing effect for the case of the ${}^7F_0 \rightarrow {}^5D_0$ transition, constituting a delicate procedure of complex magnitude. Thus, the thermometric parameter can be given by:

$$5 \quad \Delta = \frac{S({}^5D_0 \rightarrow {}^7F_2)}{S({}^5D_0 \rightarrow {}^7F_0)} e^{-\Delta E/k_B T} \quad (8)$$

where

$$\Delta E = E({}^7F_2) - E({}^7F_0). \quad (9)$$

10

Although the excitation through the 7F_2 level is highly-temperature dependent, its population practically vanishes for low temperatures and the population of the 7F_0 level no longer changes significantly, in contrast to the population of the 7F_1 . Therefore, excitation through this latter level leads to the following thermal parameter Δ' :

15

$$\Delta' = \left[\frac{n^3 \left(\frac{n^2 + 2}{3} \right)^2}{n^5} \right] \frac{S({}^5D_0 \rightarrow {}^7F_1)}{S({}^5D_0 \rightarrow {}^7F_0)} e^{-\Delta E'/k_B T} \quad (10)$$

where

$$20 \quad \Delta E' = E({}^7F_1) - E({}^7F_0). \quad (11)$$

In Eq. (10) n is the index of refraction of the material containing the Eu^{3+} ion. This index of refraction dependent term comes from the Lorentz local field correction for electric dipole and magnetic dipole absorption rates (W_{31}) when changing from absorption to spontaneous emission rates. It is crucial at this point to note that the splitting of the ${}^7\text{F}_J$ levels in a ligand field may be of the order of 300 cm^{-1} . Thus, depending on the width and peak of the excitation source, the areas and the energy differences in Eqs. (8) and (10), ΔE and $\Delta E'$, respectively, correspond to the areas of the Stark components in resonance with the excitation source.

In this work, we use nano and microcrystals of $\text{Y}_2\text{O}_3:\text{Eu}^{3+}$ as a proof of concept of the operational principles of the thermometer. $\text{Y}_2\text{O}_3:\text{Eu}^{3+}$ was chosen due to the two following reasons: i) is one of the most efficient red emitters used as a standard phosphor – absolute red emission quantum yield $>98\%$,⁴³ and ii) is chemical and photophysically stable, being synthesized as nanopowders at relatively low temperatures (*ca.* 600 K).⁴² The emission and excitation spectra of the nano and microcrystals are identical and they also coincide with the corresponding spectra of the bulk material.⁴⁴

In the Y_2O_3 matrix doped with the Eu^{3+} ion, there are two local site symmetries: C_2 and S_6 .^{42,44} Since the S_6 site has a center of inversion, it is optically inactive by the electric dipole selection rules.⁴⁵ The emission spectrum of the $\text{Y}_2\text{O}_3:\text{Eu}^{3+}$ sample (nanocrystal), in the region of the ${}^5\text{D}_0 \rightarrow {}^7\text{F}_{0,1,2}$ transitions, is shown in Fig. 2 (a). In the range corresponding to the highest intensity component of the ${}^5\text{D}_0 \rightarrow {}^7\text{F}_2$ transition, the spectrum shows that there are indeed two non-degenerate Stark components very close in energy, separated by only approximately 45 cm^{-1} , which is smaller than the width of the excitation source (135 cm^{-1}) shown in Fig. 2 (b) by the dotted line. Thus, when exciting at 611 nm, corresponding to the main peak in the ${}^5\text{D}_0 \rightarrow {}^7\text{F}_2$ transition, absorption occurs from both of these very close Stark levels. In Eq. (8), therefore, the area $S({}^5\text{D}_0 \rightarrow {}^7\text{F}_2)$ is separated in two parts given by a deconvolution (using Gaussians; see Fig. S2, Supporting Information) of the main peak

around 611 nm, each part corresponding to one Stark level. This is equivalent to taking the whole area under the emission curve, around 611 nm, including both Stark levels. In the region of the ${}^5D_0 \rightarrow {}^7F_0$ transition the second peak at 582 nm (lower energy) is assigned to a Stark component of the magnetic dipole allowed ${}^5D_0 \rightarrow {}^7F_1$ transition originated from the S_6 site.⁴² Therefore, the area $S({}^5D_0 \rightarrow {}^7F_0)$ has been obtained from a deconvolution in the wavelength region indicated by the arrow in the region around 580 nm (Fig. S3, Supporting Information).

Insert Fig.2

10

Fig. 2 (b) shows the excitation spectrum recorded at 323 and 198 K and monitoring the ${}^5D_0 \rightarrow {}^7F_4$ emission at 710 nm. The decrease of the intensity of ${}^7F_1 \rightarrow {}^5D_0$ Stark peaks (585, 593 and 597 nm) in the excitation spectrum as temperature decreases is due to the relative intra-Stark thermal population decrease. The ${}^7F_1 \rightarrow {}^5D_0$ (site S_6) peak also appears in the excitation spectrum because the Eu^{3+} ion located in the site S_6 transfers energy to the Eu^{3+} located in the site C_2 that subsequently emits.⁴² The two very close absorption Stark peaks of the 7F_2 level (herein referred to as Γ and Γ') vanish, in the excitation spectrum, at 198 K, while the absorption peak from the 7F_0 ground state increases, as expected.

Since $\Delta E = 875 \text{ cm}^{-1}$ (obtained from the energy difference between the excitation peak and the maximum in the emission spectrum in Fig.2(a)), and using the value of the areas $S({}^5D_0 \rightarrow {}^7F_2; \Gamma + \Gamma')$ and $S({}^5D_0 \rightarrow {}^7F_0)$ (Fig. S2 and Fig. S3, Supporting Information, respectively), the theoretical parameter Δ is given by:

20

$$\Delta = 51 \times \exp\left(\frac{-875}{k_B T}\right) \quad (12)$$

25

where the predicted calibration factor (the pre-exponential coefficient in Eq. (8)) is 51 and k_B is in $\text{cm}^{-1}\text{K}^{-1}$. The experimental Δ values are obtained from the integrated intensities of the ${}^5\text{D}_0 \rightarrow {}^7\text{F}_4$ transition, $S({}^5\text{D}_0 \rightarrow {}^7\text{F}_4)$, given in Figs. 3 (a) and (b). Fig. 3 (a) (excitation at 611 nm) shows that the ${}^5\text{D}_0 \rightarrow {}^7\text{F}_4$ intensity increases, with temperature, due to the increase of the thermal population of the ${}^7\text{F}_2(\Gamma+\Gamma')$ Stark levels and Fig. 3 (b) (excitation at 580 nm) shows that the ${}^5\text{D}_0 \rightarrow {}^7\text{F}_4$ intensity decreases due to the thermal depopulation of the ${}^7\text{F}_0$ ground state. For temperatures in the physiological range, Fig. 3 (c) shows the experimental thermometric values and the calculated ones using Eq. (12). The calculated values are in excellent agreement with the experimental ones. The errors (bars) were estimated by a systematic procedure. They are slightly temperature dependent. For temperatures down to 180 K the maximum error is 2%, while in the physiological region it is 3%, for Δ' and Δ , respectively.

Insert Fig.3

The performance of the thermometers can be inferred by the relative sensitivity defined by:⁴⁶

$$S_r = \frac{1}{\Delta} \left| \frac{\partial \Delta}{\partial T} \right|. \quad (13)$$

This parameter is shown for the physiological range in Fig. 3 (d). The observed values, between 1.5–1.2, are among the largest ones reported for ratiometric thermometers.¹

For temperatures down to 180 K (Eq. (10)), the excitation wavelength width, peaking around 593 nm, is not large enough to encompass the three ${}^5\text{D}_0 \rightarrow {}^7\text{F}_1$ observed Stark components (Fig. S4, Supporting Information). Once the basis line displays a non-negligible contribution to the ${}^5\text{D}_0 \rightarrow {}^7\text{F}_1$ transition intensity, we have made a deconvolution in the ${}^5\text{D}_0 \rightarrow$

7F_1 transition region and have determined the area under the 593 nm peak. The choice of this particular peak was arbitrary, and both the lower energy and higher energy Stark components could be chosen as well. In a case of very low temperature regime the lower energy component would be more appropriate. This procedure gives a calibration factor (the pre-exponential factor in Eq. (10), with a refractive index 1.6) equal to 3.6.

$$\Delta' = 3.6 \times \exp\left(\frac{-378}{k_B T}\right). \quad (14)$$

Fig. 4 (a) shows that if the 5D_0 level is excited through the 7F_1 level the intensity of the $^5D_0 \rightarrow ^7F_4$ transition increases with increasing temperature. The decrease when it is excited through the ground state is due to the thermal depopulation of this level, as expected.

Insert Fig.4

For temperatures between 180 and 290 K, Fig. 4 (c) shows the experimental thermometric values and the calculated ones using Eq. (14). As in the case of the physiological range, the calculated values are in excellent agreement with the experimental ones. Fig. 4 (d) displays the corresponding relative sensitivity. The results for the microcrystal of $Y_2O_3:Eu^{3+}$ are presented in the Supporting Information (Fig. S5 and Fig. S6, Supporting Information) and are the same as for the nanocrystal.

Conclusions

We have used thermally excited state absorption in the Eu^{3+} ion to propose a new ratiometric luminescent thermometer in which the calibration factor can be calculated from

the Eu^{3+} emission spectrum in a given compound. The thermometer is based on the temperature dependence of the ${}^5\text{D}_0 \rightarrow {}^7\text{F}_4$ emission intensity when the ${}^5\text{D}_0$ level is directly excited from specific ${}^7\text{F}_1$ or ${}^7\text{F}_2$ Stark components thermally populated with respect to the ${}^7\text{F}_0$ non degenerate ground state. For the sake of illustration of the thermometer operational principles, we have used $\text{Y}_2\text{O}_3:\text{Eu}^{3+}$ micro and nanocrystals with a relative thermal sensitivity ranging from 0.7 to 1.7 % K^{-1} (>1.2 % $\cdot\text{K}^{-1}$ in the physiological range). The thermometric system is versatile, operating in a wide range of temperature (including the physiological region) with both excitation and detection within the first biological transparency window. Furthermore, eventual quenching of the ${}^5\text{D}_0$ emitting level due to cross relaxation between Eu^{3+} ions and energy migration between them are negligible, allowing, thus, to increase the sensor concentrator up to 15–20% and, consequently, the signal-to-noise ratio. Finally, this innovative temperature sensing method permits the unprecedented prediction of the calibration factor, overcoming one of the main limitations of luminescent thermometers: the requirement of a new calibration procedure whenever the thermometer operates in a different medium (or, when not possible, the *ad hoc* assumption that a single calibration is valid independently of the medium).

Acknowledgements

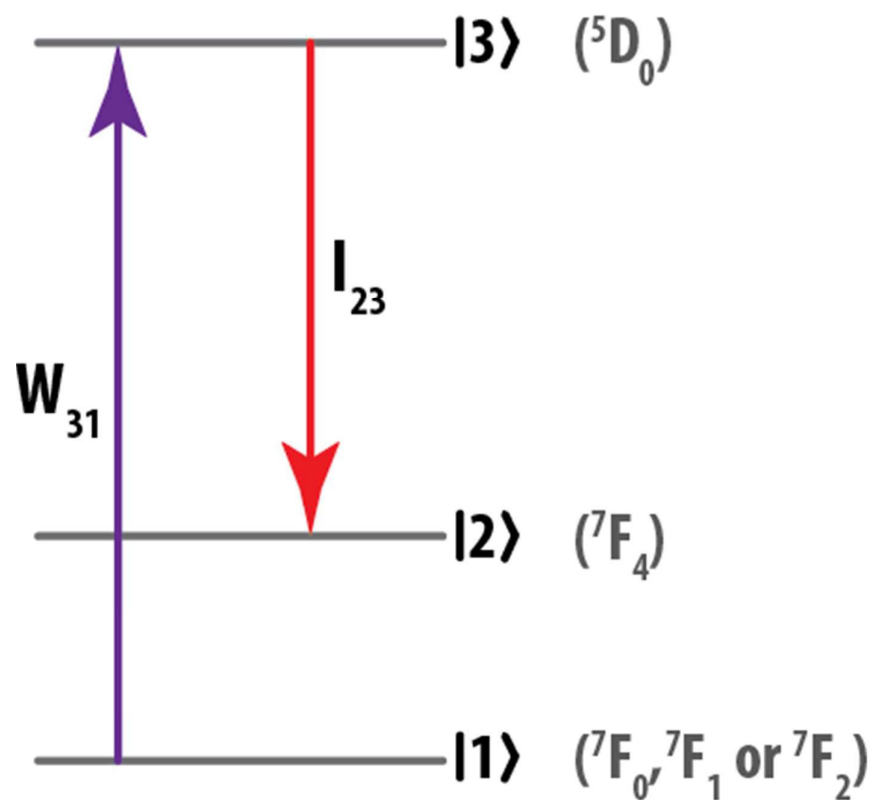
This work was developed in the scope of the project CICECO – Aveiro Institute of Materials (Ref. FCT UID /CTM /50011/2013), financed by national funds through the FCT/MEC and when applicable co-financed by FEDER under the PT2020 Partnership Agreement. LDC is grateful to CAPES and CNPq (Brazil) for a fellowship within the science without borders program.

References

1. C. D. S. Brites, P. P. Lima, N. J. O. Silva, A. Millán, V. S. Amaral, F. Palacio and L. D. Carlos, *Nanoscale*, 2012, **4**, 4799-4829.
- 5 2. X. D. Wang, O. S. Wolfbeis and R. J. Meier, *Chem. Soc. Rev.*, 2013, **42**, 7834-7869.
3. D. Jaque and F. Vetrone, *Nanoscale*, 2012, **4**, 4301-4326.
4. L. Shi, C. Dames, J. R. Lukes, P. Reddy, J. Duda, D. G. Cahill, J. Lee, A. Marconnet, K. E. Goodson, J.-H. Bahk, A. Shakouri, R. S. Prasher, J. Felts, W. P. King, B. Han and J. C. Bischof, *Nanosc. Microsc. Therm.*, 2015, **19**, 127-165.
- 10 5. M. Mecklenburg, W. A. Hubbard, E. R. White, R. Dhall, S. B. Cronin, S. Aloni and B. C. Regan, *Science*, 2015, **347**, 629-632.
6. K. Okabe, N. Inada, C. Gota, Y. Harada, T. Funatsu and S. Uchiyama, *Nat. Commun.*, 2012, **3**, 705.
7. D. Jaque, B. del Rosal, E. M. Rodriguez, L. M. Maestro, P. Haro-Gonzalez and J. G. Solé, *Nanomedicine*, 2014, **9**, 1047-1062.
- 15 8. C. D. S. Brites, P. P. Lima, N. J. O. Silva, A. Millán, V. S. Amaral, F. Palacio and L. D. Carlos, *Adv. Mater.*, 2010, **22**, 4499-4504.
9. H. Peng, M. I. Stich, J. Yu, L. N. Sun, L. H. Fischer and O. S. Wolfbeis, *Adv. Mater.*, 2010, **22**, 716-719.
- 20 10. Y. Cui, H. Xu, Y. Yue, Z. Guo, J. Yu, Z. Chen, J. Gao, Y. Yang, G. Qian and B. Chen, *J. Am. Chem. Soc.*, 2012, **134**, 3979-3982.
11. U. Rocha, C. Jacinto da Silva, W. Ferreira Silva, I. Guedes, A. Benayas, L. Martínez Maestro, M. Acosta Elias, E. Bovero, F. C. van Veggel, J. A. García Solé and D. Jaque, *ACS Nano*, 2013, **7**, 1188-1199.
- 25 12. V. Lojpur, G. Nikolic and M. D. Dramicanin, *J. Appl. Phys.*, 2014, **115**, 203106.
13. R. Piñol, C. D. Brites, R. Bustamante, A. Martínez, N. J. Silva, J. L. Murillo, R. Cases, J. Carrey, C. Estepa, C. Sosa, F. Palacio, L. D. Carlos and A. Millán, *ACS Nano*, 2015, **9**, 3134-3142.
14. E. Hemmer, M. Quintanilla, F. Legare and F. Vetrone, *Chem. Mater.*, 2015, **27**, 235-244.
- 30 15. Z. P. Wang, D. Ananias, A. Carne-Sanchez, C. D. S. Brites, I. Imaz, D. MasPOCH, J. Rocha and L. D. Carlos, *Adv. Funct. Mater.*, 2015, **25**, 2824-2830.
16. R. A. S. Ferreira, C. D. S. Brites, C. M. S. Vicente, P. P. Lima, A. R. N. Bastos, P. G. Marques, M. Hiltunen, L. D. Carlos and P. S. André, *Laser Photonics Rev.*, 2013, **7**, 1027-1035.
- 35 17. A. Benayas, B. del Rosal, A. Perez-Delgado, K. Santacruz-Gomez, D. Jaque, G. A. Hirata and F. Vetrone, *Adv. Opt. Mater.*, 2015, **3**, 687-694.
18. C. D. S. Brites, P. P. Lima, N. J. O. Silva, A. Millán, V. S. Amaral, F. Palacio and L. D. Carlos, *Nanoscale*, 2013, **5**, 7572-7580.
19. M. Homma, Y. Takei, A. Murata, T. Inoue and S. Takeoka, *Chem. Commun.*, 2015, **51**, 6194-6197.
- 40 20. Y. Takei, S. Arai, A. Murata, M. Takabayashi, K. Oyama, S. Ishiwata, S. Takeoka and M. Suzuki, *ACS Nano*, 2014, **8**, 198-206.
21. J. S. Donner, S. A. Thompson, M. P. Kreuzer, G. Baffou and R. Quidant, *Nano Lett.*, 2012, **12**, 2107-2111.
- 45 22. C. Gota, S. Uchiyama and T. Ohwada, *Analyst*, 2007, **132**, 121-126.
23. C. Gota, K. Okabe, T. Funatsu, Y. Harada and S. Uchiyama, *J. Am. Chem. Soc.*, 2009, **131**, 2766-2767.

24. C. Pietsch, U. S. Schubert and R. Hoogenboom, *Chem. Commun.*, 2011, **47**, 8750-8765.
25. L. M. Maestro, Q. Zhang, X. Li, D. Jaque and M. Gu, *Appl. Phys. Lett.*, 2014, **105**, 181110.
- 5 26. L. H. Fischer, G. S. Harms and O. S. Wolfbeis, *Angew. Chem.-Int. Edit.*, 2011, **50**, 4546-4551.
27. M. L. Debasu, D. Ananias, I. Pastoriza-Santos, L. M. Liz-Marzán, J. Rocha and L. D. Carlos, *Adv. Mater.*, 2013, **25**, 4868-4874.
28. Y. Huang, F. Rosei and F. Vetrone, *Nanoscale*, 2015, **7**, 5178-5185.
- 10 29. O. A. Savchuk, P. Haro-Gonzalez, J. J. Carvajal, D. Jaque, J. Massons, M. Aguilo and F. Diaz, *Nanoscale*, 2014, **6**, 9727-9733.
30. S. J. Cho, D. Maysinger, M. Jain, B. Roder, S. Hackbarth and F. M. Winnik, *Langmuir*, 2007, **23**, 1974-1980.
31. A. Gnach, T. Lipinski, A. Bednarkiewicz, J. Rybka and J. A. Capobianco, *Chem. Soc. Rev.*, 2015, **44**, 1561-1584.
- 15 32. H. Kusama, O. J. Sovers and T. Yoshioka, *Jpn. J. Appl. Phys.*, 1976, **15**, 2349-2358.
33. M. A. R. C. Alencar, G. S. Maciel, C. B. de Araújo and A. Patra, *Appl. Phys. Lett.*, 2004, **84**, 4753-4755.
- 20 34. F. Vetrone, R. Naccache, A. Zamarron, Á. J. de la Fuente, F. Sanz-Rodriguez, L. M. Maestro, E. M. Rodriguez, D. Jaque, J. G. Solé and J. A. Capobianco, *ACS Nano*, 2010, **4**, 3254-3258.
35. M. Bettinelli, L. D. Carlos and X. Liu, *Phys. Today*, 2015, **68**.
36. D. Wawrzynczyk, A. Bednarkiewicz, M. Nyk, W. Strek and M. Samoc, *Nanoscale*, 2012, **4**, 6959-6961.
- 25 37. U. Rocha, K. U. Kumar, C. Jacinto, J. Ramiro, A. J. Caamano, J. G. Solé and D. Jaque, *Appl. Phys. Lett.*, 2014, **104**, 053703.
38. E. Carrasco, B. del Rosal, F. Sanz-Rodríguez, Á. J. de la Fuente, P. H. Gonzalez, U. Rocha, K. U. Kumar, C. Jacinto, J. G. Solé and D. Jaque, *Adv. Funct. Mater.*, 2015, **25**, 615-626.
- 30 39. S. Balabhadra, M. L. Debasu, C. D. S. Brites, L. A. O. Nunes, O. L. Malta, J. Rocha, Marco Bettinelli and L. D. Carlos, *Nanoscale*, 2015, 10.1039/C1035NR05631D.
40. Y. Liu, G. D. Qian, Z. Y. Wang and M. Q. Wang, *Appl. Phys. Lett.*, 2005, **86**.
41. J. Silver, M. I. Martinez-Rubio, T. G. Ireland, G. R. Fern and R. Withnall, *J. Phys. Chem. B*, 2001, **105**, 9107-9112.
- 35 42. I. G. N. Silva, L. C. V. Rodrigues, E. R. Souza, J. Kai, M. C. F. C. Felinto, J. Holsa, H. F. Brito and O. L. Malta, *Opt. Mater.*, 2015, **40**, 41-48.
43. G. Blasse and B. C. Grabmaier, *Luminescent Materials*, Springer-Verlag, Berlin, 1994.
44. M. Buijs, A. Meyerink and G. Blasse, *J Lumin*, 1987, **37**, 9-20.
45. O. L. Malta, E. Anticfidancev, M. Lemaitreblaise, A. Milicictang and M. Taibi, *J. Alloy. Compd.*, 1995, **228**, 41-44.
- 40 46. S. Collins, G. Baxter, S. Wade, T. Sun, K. Grattan, Z. Zhang and A. Palmer, *J. Appl. Phys.*, 1998, **84**, 4649-4654.

Figures and Tables



- 5 **Fig. 1.** Schematic energy level diagram used to simulate the energy levels of the Eu^{3+} ion involved in the thermometer operation.

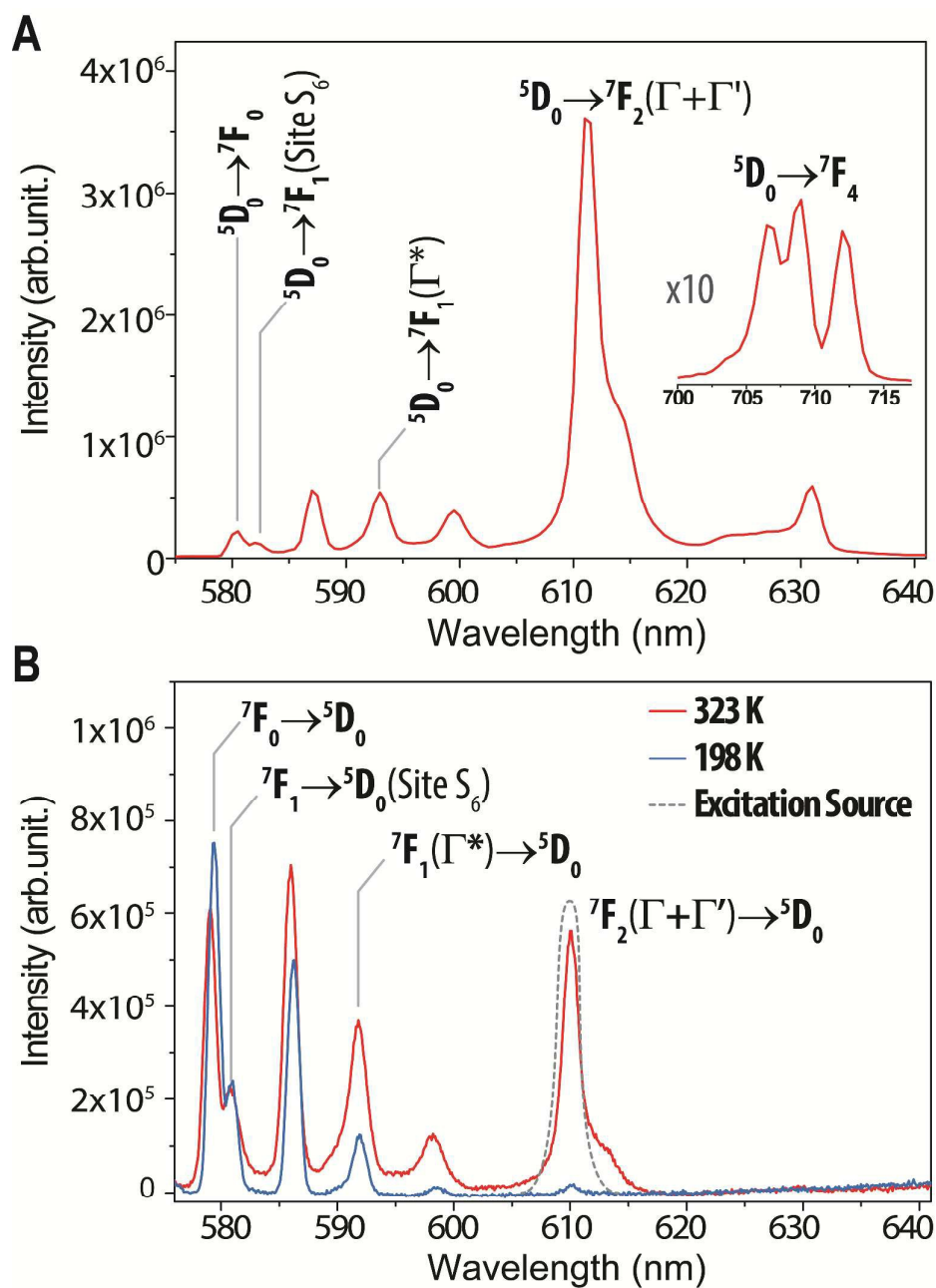


Fig. 2. (A) Emission spectrum of the $\text{Y}_2\text{O}_3:\text{Eu}^{3+}$ nanocrystals under 396 nm excitation and at 300 K. The inset shows the emission in the range 690-715 nm of the $^5\text{D}_0 \rightarrow ^7\text{F}_4$ transition. (B) Excitation spectra of the $\text{Y}_2\text{O}_3:\text{Eu}^{3+}$ nanocrystals, at 323 K (blue line) and at 198 K (black line) monitored at 710 nm ($^7\text{F}_4$ manifold). Dotted line is the profile of the excitation source.

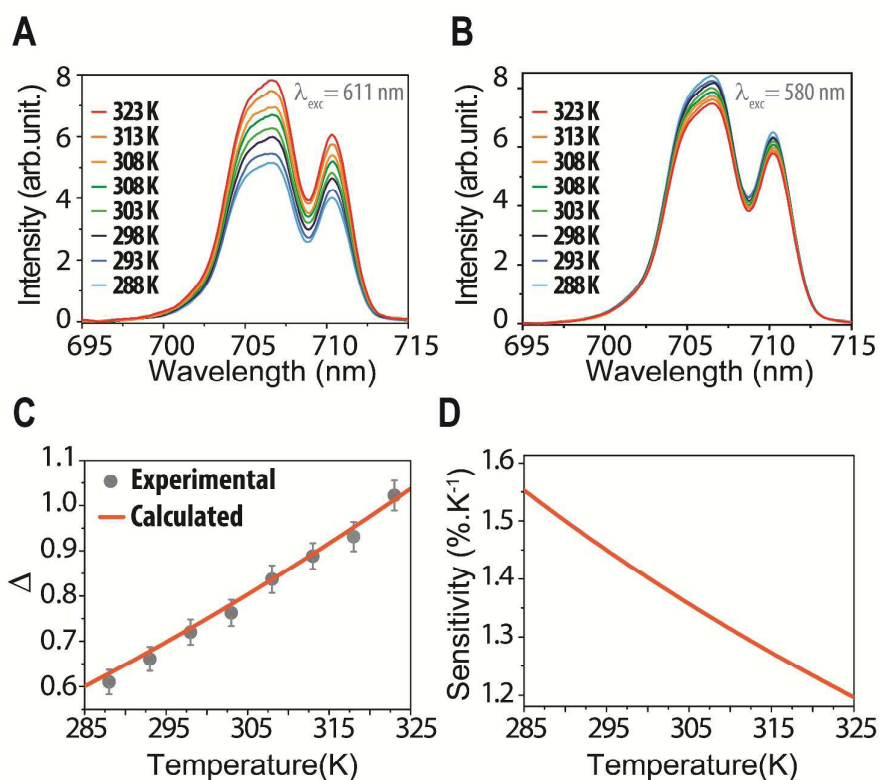


Fig. 3. Emission spectra of the $\text{Y}_2\text{O}_3:\text{Eu}^{3+}$ nanocrystals in the range 690–715 nm of the $^5\text{D}_0 \rightarrow$
 5 $^7\text{F}_4$ transition exciting at (A) 611 nm and (B) 580 nm. (C) Thermometric parameter for the
 physiological range. Points are the experimental values of the Δ parameter obtained from the
 spectra in (A) and (B) after being corrected for the respective excitation intensity, whereas the
 line is the calculated curve obtained from Eq. (12). The error bars in the thermometric
 parameter are calculated at each temperature. (D) Relative sensitivity in the physiological
 10 range.

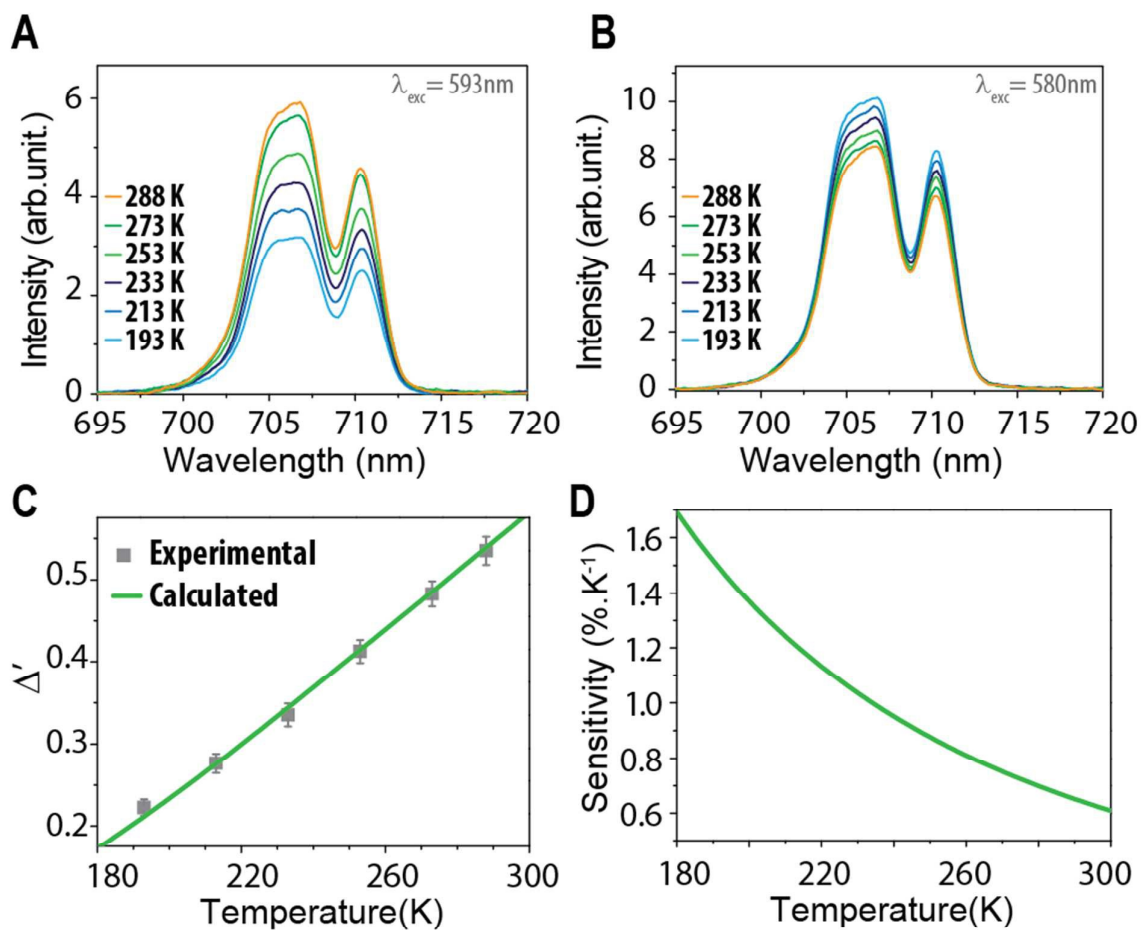


Fig. 4. The same as in Fig. 3 for the lower temperature range (exciting at 593 nm, 7F_1 (Δ')

5 level).